Title

Dynamic Pressure Technique for Estimating Permeability and Anisotropy of Soil to Air Flow Over a Scale of Several Meters

Authors

Garbesi, K.
Sextro, R.G.
Nazaroff, W.W.

Publication Date

1992-09-01

LBL-32723
UC-402
Preprint

Lawrence Berkeley Laboratory
UNIVERSITY OF CALIFORNIA

ENERGY & ENVIRONMENT DIVISION

Submitted to Environmental Science and Technology

A Dynamic Pressure Technique for Estimating Permeability and Anisotropy of Soil to Air Flow Over a Scale of Several Meters

K. Garbesi, R.G. Sextro, and W.W. Nazaroff

September 1992

ENERGY & ENVIRONMENT DIVISION

Prepared for the U.S. Department of Energy under Contract Number DE-AC03-76SF00098

DISCLAIMER

LBL-32723

Submitted to *Environmental Science and Technology*

A DYNAMIC PRESSURE TECHNIQUE FOR ESTIMATING PERMEABILITY AND ANISOTROPY OF SOIL TO AIR FLOW OVER A SCALE OF SEVERAL METERS

Karina Garbesi, Richard G. Sextro, and William W. Nazaroff

October 1992

Indoor Environment Program
Energy and Environment Division
Lawrence Berkeley Laboratory
1 Cyclotron Road
Berkeley, California 94720

This work was supported by the Director, Office of Energy Research, Office of Health and Environmental Research, Environmental Sciences Division, and by the Assistant Secretary for Conservation and Renewable Energy, Office of Building and Community Systems, Building Systems and Materials Division of the U.S. Department (DOE), under Contract DE-AC03-76SF00098.

Abstract

An technique was developed to measure the effective permeability of soil to air on a scale of several meters. A sinusoidally oscillating pressure signal, imposed at a source probe, is recorded at a detector probe. The time lag between the imposed and detected signals is used to determine the effective permeability along the path between the probes. The technique improves upon previous methods by offering relatively unweighted and longer integration paths. It also allows the detection of anisotropy in permeability. A field test of the dynamic pressure technique suggests that soil permeability at the test site depends upon sampling scale—an indication that the use of multiple small-scale measurements to characterize regional soil permeabilities can produce significantly misleading results. The field experiment also indicated the presence of horizontal-vertical anisotropy, with horizontal permeability exceeding vertical by a factor of 1.7.

Introduction

For a number of applications it is desirable to characterize the permeability of soil to air over path lengths of several meters. This is the scale at which houses tend to interact with the surrounding soil, drawing in soil-gas-borne contaminants such as radon and volatile organic compounds. That scale is approximately determined by the distance between the soil surface (the source of air entering the soil) and entry points of soil-gas into the house, such as gaps or cracks in the building substructure or permeable substructure walls. This can also be a useful scale over which to study the characteristics of the unsaturated zone above contaminated ground water or a free-liquid plumes.

Field studies of the entry of radon and VOC into houses have characterized soil permeability using static techniques that impose a constant flow of air through a soil probe. Permeability is inferred from the known flow rate and from measurements of the pressure difference between the probe and the soil surface.(1-4) Because of practical constraints on the probe size, integration of the information about soil permeability is limited to a relatively small distance from source (~0.1-0.5 m radius).(5)

To determine regional soil permeabilities for input to soil-gas transport models, many of these small-scale measurements are typically averaged together. Persistent discrepancies between modeled and measured soil-gas and radon entry rates into houses has suggested that small-scale measurements might not reflect soil characteristics at the larger scales at which houses typically interact with soils.(4) It is therefore desirable to have a measurement technique that integrates on such scales, that can be used *in situ* with minimal disturbance to the soil.

Anisotropy of the permeability of the soil to air due to small-scale structure--or effective anisotropy due to the presence of larger-scale, homogeneous isotropic layers with distinct permeabilities--is another possible confounding factor in predicting gas-phase contaminant transport through soils. Nazaroff et al. (6) and Garbesi and Sextro (1) describe two studies in which large discrepancies between measured and modeled pressure coupling between a house and the surrounding soil were believed to be explained by soil layering. Anisotropy can produce the same effect, spreading the pressure field in the horizontal direction if horizontal permeabilities are higher than vertical permeabilities.

Laboratory methods exist for determining anisotropy from field samples.(7) However, these methods have serious limitations in the applications mentioned because of the inherent problem of maintaining sample integrity during the sampling and measurement process, and the need for a large number of samples to determine soil characteristics over the desired scale. Tanner (8) developed a soil probe specifically for the measurement of soil anisotropy. As in the case of other static measurements described above, the probe imposes a localized steady pressure that intrinsically weights information about soil conditions to the near-probe soil. In addition, with a single probe it is not possible to determine the orientation of the anisotropy.

To overcome these limitations, we have developed a dynamic technique for measuring soil permeabilities over a scale of several-meters. The technique uses a known sinusoidal pressure oscillation imposed at one probe that is detected at a second probe. The time lag between the source and detector signals is used to determine the effective permeability of the path between the probes. By varying the location of the detector probe, one can detect anisotropy in soil permeability, or effective anisotropy due to soil layering, aong any arbitrary path. This paper presents the theoretical development of the method and demonstrates its application at a site with natural soil that is used for the study of radon entry into houses.

Theory

Model Development:
We use a mass balance for soil air to derive the mathematical description of three-dimensional propagation of a pressure signal in soil. For a representative volume element of soil, with dimensions $\Delta x \Delta y \Delta z$ and air-filled porosity ε. The change in the mass of air in the volume that occurs over a time Δt must equal the mass entering the volume minus the mass leaving the volume in the same time increment. Given soil gas velocities in the x, y, and z directions, v_x, v_y, and v_z, respectively, this relationship is described by

$$\Delta P(x,y,z)(\Delta x\Delta y\Delta z)\frac{\varepsilon M}{RT} = v_x(x,y,z)(\Delta y\Delta z\Delta t)\rho + v_y(x,y,z)(\Delta x\Delta z\Delta t)\rho$$

(1) $$+v_z(x,y,z)(\Delta x\Delta y\Delta t)\rho - v_x(x+\Delta x,y,z)(\Delta y\Delta z\Delta t)\rho - v_y(x,y+\Delta y,z)(\Delta x\Delta z\Delta t)\rho$$
$$-v_z(x,y,z+\Delta z)(\Delta x\Delta y\Delta t)\rho$$

where ΔP is the change in pressure induced by the change in mass, M is the molar weight of air, R is the universal gas constant, T is the temperature, and ρ is the density of the air. The velocities are given as volumetric flow through total cross sectional area of the soil volume element. We consider changes in density small enough that ρ can be considered constant. That is, the pressure fluctuations are small relative to the ambient pressure.

Dividing (1) by $\rho\Delta x\Delta y\Delta z\Delta t$, and taking the limit as Δx, Δy, Δz, and Δt approach zero:

(2) $$\frac{\varepsilon M}{\rho RT}\frac{\partial P}{\partial t} = -\frac{\partial v_x}{\partial x} - \frac{\partial v_y}{\partial y} - \frac{\partial v_z}{\partial z} = -\nabla \cdot \mathbf{v}$$

We assume that flow is governed by Darcy's law. The x, y, and z components of velocity are then given by:

(3a) $$v_x = \frac{-k_x}{\mu}\frac{\partial P}{\partial x}$$

(3b) $$v_y = \frac{-k_y}{\mu}\frac{\partial P}{\partial y}$$

(3c) $$v_z = \frac{-k_z}{\mu}\frac{\partial P}{\partial z}$$.

In general, in the three dimensional case, permeability is described by a 3x3 tensor. We have made the assumption here that our Cartesian coordinate axes are aligned with the principle directions of anisotropy--that is that we have horizontal/vertical anisotropy. This has the effect of diagonalizing the tensor, giving the result in Equation 3.

Darcy's law requires that the Reynolds number, based on average grain diameter, does not exceed some number between one and 10 ((9), p. 126), consistent with our requirement of small pressure oscillations. Equation 3 indicates the x, y, and z components of velocity corresponding to soil permeabilities k_x, k_y, and k_z, in each of these directions, and μ is the dynamic viscosity of the air. Substituting Equations 3a - c into Equation 2 we obtain the differential equation as a function of pressure:

$$(4) \qquad \frac{\partial P}{\partial t} = \frac{1}{\varepsilon\mu}\frac{\rho RT}{M}\left(\frac{\partial}{\partial x}\left(k_x\frac{\partial P}{\partial x}\right)+\frac{\partial}{\partial y}\left(k_y\frac{\partial P}{\partial y}\right)+\frac{\partial}{\partial z}\left(k_z\frac{\partial P}{\partial z}\right)\right) .$$

To obtain an analytical solution, we assume that the soil permeabilities in the x, y, and z direction are constant and equal (*i.e.*, homogeneous and isotropic). Recognizing that ($\rho RT/M$) is simply the average atmospheric pressure, P_o, Equation 4 becomes:

$$(5) \qquad \frac{\partial P}{\partial t} = D_p \nabla^2 P ,$$

which is simply the diffusion equation for pressure propagation with a diffusion constant

$$(6) \qquad D_p = \frac{kP_o}{\varepsilon\mu} .$$

We will use the homogeneous isotropic model to interpret our probe-to-probe measurements of soil permeability, and for first order estimation of soil anisotropy. It makes sense to use such a model when characterizing unknown soils since there is no way of knowing *a priori* what the macroscopic soil geometry is. Furthermore, if heterogeneity occurs on a relatively small scale and is randomly distributed, these assumptions will not introduce a bias into the results. Systematic heterogeneity (*e.g.*, soil layering) or anisotropy can bias the results. In which case a more accurate description of the soil could be obtained by iterating the result against a numerical model that incorporates the guessed soil structure characteristics and comparing the output of the model with the measurements. The advantage of the current technique is that anisotropy can be unambiguously detected and a first order estimate obtained. With this knowledge one can then make the judgment as to whether it is desirable to do the extra work to get more precise results.

For this theoretical derivation, we consider a pressure source at a spherical surface, r = b. We begin the analysis by considering the case of a source buried in an infinite homogeneous medium. This system is spherically symmetric, so we can consider the disturbance pressure P to be a function of r and t alone. The initial and boundary conditions for Equation 5 are:

(7.a)	$P(r,0) = 0$	for $r \geq b$
(7.b)	$P(b,t) = P_a \sin(\omega t)$	for $t > 0$
(7.c)	$P(r \rightarrow \infty,t) = 0$	for $t > 0$

In spherical coordinates, Equation 5 can be rewritten:

(8) $$\frac{\partial P}{\partial t} = D_p \frac{1}{r^2}\frac{\partial}{\partial r}\left(r^2 \frac{\partial P}{\partial r}\right).$$

We make the transformation

(9) $$W(r,t) = r\,P(r,t)$$

to obtain a one-dimensional partial differential equation of the form:

(10) $$\frac{\partial W}{\partial t} = D_p \frac{\partial^2 W}{\partial r^2},$$

with the transformed initial and boundary conditions

(11a) $W(r,0) = 0$ for $r \geq b$

(11.b) $W(b,t) = b\,P_a \sin(\omega t)$ for $t > 0$

(11.c) $W(\infty,t) = 0$. for $t > 0$

A solution to this problem may be found by applying Duhamel's method to the solution of the same problem with a step function boundary condition, W(b,t)=1.((10), pg. 30-31) That solution is obtained by Laplace transform as:

(12) $$\Phi(r,t) = \frac{2}{\sqrt{\pi}} \int_{\frac{r-b}{\sqrt{4Dt}}}^{\infty} e^{\xi^2} d\xi.$$

And the complete solution is:

(13) $$W(r,t) = \int_0^t W(b,\tau)\frac{\partial}{\partial t}\Phi(r,t-\tau)d\tau$$

Taking the derivative of Equation 12, this gives:

(14) $$W(r,t) = \int_0^t W(b,\tau)\frac{(r-b)}{(t-\tau)}\frac{e^{-\frac{(r-b)^2}{4D_p(t-\tau)}}}{\sqrt{4\pi D_p(t-\tau)}}d\tau \quad .$$

Or, in terms of the original quantities:

(15) $$P_R(r,t) = \frac{1}{r}\int_0^t bP_a \sin(\omega\tau)\frac{(r-b)}{(t-\tau)}\frac{e^{-\frac{(r-b)^2}{4D_p(t-\tau)}}}{\sqrt{4\pi D_p(t-\tau)}}d\tau.$$

The subscript R on P indicates that the solution is for a point a distance r away from the center of the real source (R) located in the infinite medium.

We now consider the effect of the boundary condition at the soil surface. Because we are imposing a distinctive signal at the source probe that can be detected unambiguously at the detector probe, we can ignore barometric pressure fluctuations at the soil surface, and consider the pressure there constant. The barometric pressure fluctuations average to zero over the course of the experiment, so our boundary condition is taken as P(surface,t) = 0.

The method of images is used to capture the effect of the zero pressure boundary at the soil surface (see for example (11), p.12). Figure 1 shows the geometry for the real and image sources and two possible probe locations. The distances between the real and image sources and the detector probe are r and r', respectively. The response to the image source at the probe location is:

$$(16) \qquad P_I(r',t) = -\frac{1}{r'}\int_0^t bP_a \sin(\omega\tau)\frac{(r'-b)}{(t-\tau)}\frac{e^{-\frac{(r'-b)^2}{4D_p(t-\tau)}}}{\sqrt{4\pi D_p(t-\tau)}}d\tau$$

The solution in the finite domain bounded above by the soil surface is obtained by adding Equations 15 and 16, to give the time-dependent signal ($P_{det}(t)$) at the detector location:

$$(17) \qquad P_{det}(t) = P_R(r,t) + P_I(r',t) \ .$$

Model Application:
In practice, Equations 15 and 16 are integrated numerically for a series of t and fixed distances, r and r', using commercially available numerical analysis software (MathCad, MathSoft Inc., Cambridge, MA). The results are added together to find the predicted pressure as a function of time at the detector location. The result is a phase-shifted and attenuated sinusoidal signal that grows in to its stable time-dependent signature over a period r^2/D--the step function response time of the system. After that time the signal is a non-trending, stable sinusoid at the driving frequency. The phase of the stable detector signal is then compared to that of the source to determine the total time for a given trough to travel from the source to the detector. This is called the lag time.

Figure 2 shows a sample set of theoretical curves of lag time vs. permeability for a source signal with a 60 s period imposed at 2-m depth. Each figure shows traces for a number of possible detector locations, identified by their radial distance from the source (r) and angle (θ), as in Figure 1. The following

parameters are used in the calculations to correspond with conditions in the field test:

(18.a)	P_a	= 900 Pa	Amplitude of the driving signal.
(18.b)	T	= 60 s	Period of the driving signal.
(18.c)	ω	= $2\pi/T$ s^{-1}	Frequency of driving signal.
(18.d)	P_o	= 92,000 Pa	Mean atmospheric pressure at experiment site.
(18.e)	μ	= 1.8×10^{-5} Pa s	Dynamic viscosity of air.
(18.f)	b	= 0.1 m	Effective spherical radius of source.
(18.g)	ε	= 0.45±.02	Air-filled porosity of soil.

The air-filled porosity is calculated from the absolute porosity reported in (12), and from soil moisture content measured using a time domain reflectometer devise (Trase, System 1, Soilmoisture Equipment Corp., Santa Barbara, CA).

The driving frequency can be optimized for specific soil conditions. Higher frequency driving signals allow measurements to be made in a shorter amount of time but produce lower amplitude detector signals.

The phase shift at the detector location depends on the frequency of the imposed signal. This agrees with the analytical solution for the one-dimensional case.(13) We checked our theoretical solution by carrying out the same dynamic pressure measurement at two different driving periods, 30 and 60 s. The two different lag times observed experimentally yielded the same estimates of permeability when compared to the appropriate theoretical trace.

Experiment

Experimental Design:
To test the dual-probe dynamic pressure technique, we made measurements at a site currently being used for the study of radon entry into an experimental basement(4, 14). Spot measurements of soil permeability were made at the site using both blunt-end soil probes (technique described in (15)) and probes through which sampling occurs near the end of a sealed steel pipe via a welded-in cylindrical well screen. (Technique described in (5) and results in (4)).

The source probe used in this experiment was a previously installed well-screen probe, oriented horizontally and lying 2 m below the soil surface and 5-m south of the structure. This probe was used because the well screen provides a large enough surface area to the soil to propagate the pressure signal through several meters of soil without excessive signal loss due to attenuation, while maintaining soil-gas velocity well within the Darcy limit at a distance 0.01 m from the source. The effective spherical radius of the cylindrical source was determined by comparing a numerical simulation of a static pressure field around a cylindrical

source with the analytical prediction of the field surrounding a spherical source. An effective spherical radius of 0.10 m was estimated for the 15-cm-long well screen. The maximum error associated with the spherical-source approximation can be determined from consideration of the real and approximated sources. The maximum distance between the surfaces of the real 0.01-m radius cylindrical source and the assumed 0.1-m spherical source is 0.04 m. For a pressure signal propagating at constant velocity along a 2-m path, this represents error in the lag time of 0.04/2, or 2%. From Figure 2, for a 2-m probe at 0°, this would produce an uncertainty in permeability of only about 1%.

Six detector probes were installed vertically from the soil surface using a procedure described previously(2). Each probe consisted of an open-ended length of 10-mm ID galvanized steel pipe (nominally 1/8-inch) threaded at the top for connection to 4-mm ID polyethylene tubing. The tubing carried the pressure signal to a low-range, variable reluctance pressure transducer (resolution ~ 0.2 Pa). Figure 3 shows the spatial distribution of the source and detector probes. Each of the six detector probes terminated at a radial distance of 2 m from the source. Three of the probes sampled from the same depth as the source probe ($r = 2$ m, $\theta = 0°$, Figure 1), the other three sampled the near-surface soil ($r = 2$ m, $\theta = 45°$, Figure 1). Two previously installed well-screen probes were also used for signal detection, one with $r=2.69$ m and $\theta = 0°$, the other with $r = 3.12$ m and $\theta = 30°$. To avoid undue disturbance of the pressure field at the probe tip due to compaction of soil during probe installation, the soil at the bottom of each blunt-end probe was loosened using a wood auger welded to the end of a long rod.

The driving signal was created using two mass flow controllers coupled as shown in Figure 4. To create a sinusoidally oscillating pressure signal centered about mean atmospheric pressure, one mass flow controller was driven to produce a sinusoidal flow with a positive DC offset ($Q = A \sin(\omega t)$), while the other maintained a constant negative offset of the same amplitude ($Q = -A$). The flows were 'tuned' at the site to produce a source pressure amplitude of about 900 Pa.

Before the start of each experiment the sinusoidally oscillating source flow was vented to atmosphere. The source probe was also open to atmosphere to ensure neutral pressure. While recording the pressure signal at the source and detector probes, at $t = 0$, the source signal was switched to the source probe. Data were collected for about 20 minutes. We found that it was sufficient to gather about 20 driving-frequency cycles to get a good signal to noise ratio. For the soil we investigated, driving periods between 30 and 60 s were optimal. For low permeability soils, however, one might want to use a lower driving frequency to increase the amplitude of the detected signal, and to integrate longer to reduce the effect of noise. Laboratory tests ensured that phase shift and amplitude attenuation of the signal across the length of tubing and probe was negligible.

These same tests demonstrated that there were no problems due to potentially different response times of the source and detector pressure transducers.

Data Analysis:
The source and detector signals were decomposed into their frequency components by Fast Fourier Transform (FFT) using commercially available software (MathCad, MathSoft Inc., Cambridge, MA) running on an IBM PC clone with 2 Mb RAM. A peak at the driving frequency was clearly visible in all of our detector signals. The phase information from the FFT was then used to determine the lag time between the source and detector signals. In our case, visual inspection of the raw data was sufficient to ascertain that the first peak arrived at the detector within the first source signal period rather than during some later period, in which case the actual lag time would be some integral multiple of the period plus the lag determined by the transform.

A combination of two factors, numerical dispersion and environmental noise, makes it advantageous to use lag time rather than amplitude attenuation of the source signal as the indicator of permeability. Numerical execution of the FFT on even a pure, single-frequency, sinusoidal data train of finite length shows that there can be considerable dispersion of the signal into adjacent frequency bands. When environmental noise is added to the detected signal, it becomes impossible to determine how much of the power in adjacent bands actually belongs to the driving signal and how much results from real noise. Therefore, the amplitude at the driving frequency is largely uncertain.

The lag time, on the other hand, is determined by comparison of the source and detector signals at the driving frequency alone, and the resolution of the signal is determined only by the number of data points collected and the sampling frequency. Furthermore, lag times give better resolution at large distances from the source because the propagation velocity changes less rapidly with distance from the source than does the signal amplitude.

Results:
The results of the probe-to-probe dynamic permeability measurements are displayed in square brackets in Figure 3 for each source-to-detector path. The permeabilities measured at each of the probes using the static technique are shown in parentheses. Table I lists the permeabilities and indicates the ratio of the dynamic result for each path to the average of the static measurements at its end points. The uncertainty in the results of the dynamic pressure measurements are determined by the uncertainty in the measurement of air-filled porosity and the uncertainty in the measured lag time, which are about comparable.

Two observations stand out: (1) The dynamic measurements consistently give a higher estimate of permeability than the static measurements, a factor of six, on average. This appears to indicate that permeability is scale-dependent--effective permeability increasing with increasing sampling scale. The results of the

measurements on the N-D and N-M probes support this finding--these are the longest probes and they have the highest observed permeabilities. (2) The dynamic measurements also yield consistently higher permeabilities for the horizontal than vertical direction indicating the presence of anisotropy. As expected, the dynamic results are considerably less variable than the static results because sampling occurs over a longer integration path, minimizing the detection of small-scale heterogeneity.

A first order approximation of vertical-horizontal anisotropy can be made using the hydrogeological concept of a hydraulic-conductivity ellipse.((16), p. 174). The data suggest that we have one horizontal permeability, k_h, and one vertical permeability, k_v, so we can do the analysis in two dimensions. The permeability ellipse is given by:

$$\frac{x^2}{k_h} + \frac{z^2}{k_v} = 1 \tag{19}$$

The measurement made at $\theta = 45^o$ gives us the location of a point on the ellipse at:

$$x = z = \sqrt{k_{45^o}}\cos(45^\circ) \tag{20}$$

From the data in Table I, the average estimate of horizontal permeability (k_h), based on the 2-m long, $\theta = 0$, detector probes, is 23×10^{-12} m^2. The average permeability along $\theta = 45^o$ (k_{45}) is 17×10^{-12} m^2. Using these values and substituting Equation 20 into Equation 19, k_v is estimated to be 14×10^{-12} m^2, 0.6 times the horizontal value.

Discussion

Dynamic measurements of soil permeability to air have been made previously.(13, 17, 18) These measurements used fluctuations in barometric pressure as the source signal and were confined to assessments of vertical permeabilities. Dependence upon the vicissitudes of the barometric pressure signal limits the range of soil conditions and physical scales over which measurements can be made using this one-dimensional technique, and complicates data analysis, creating large uncertainties in estimates of permeability.(18)

In contrast, the use of a controlled sinusoidal source signal in the current technique enables precise, phase-sensitive detection with low uncertainty. Signal amplitude and period can be adjusted for detection over longer paths or in lower permeability soil. In cases of high environmental noise, signals can be

integrated over arbitrarily long times, limited only by the size of RAM in the computer doing the FFT. This is not a serious limitation with the current availability of inexpensive computing power.

One of the desirable features of this measurement technique is that the results do not contain the 1/r weighting factor inherent in small-source static techniques (that mirrors the 1/r fall off of the static pressure field). The difference derives from our use of the wave-front propagation time as the parameter to determine permeability. In an infinite homogeneous and isotropic medium, the propagation velocity is constant, independent of distance from the source. To the extent that this is true for our semi-infinite medium, we obtain unweighted results from our dual-probe technique, with each point along the path contributing equally to the characterization.

To explore the effect of the semi-infinite medium on the weighting factor, we plot the time lag of the source-to-detector signal with radial distance from the source as the signal propagates in the vertical and horizontal directions. Figures 5a and b show the results for two different soils with homogeneous permeabilities of 8.5×10^{-13} m^2 and 8.5×10^{-12} m^2, respectively. When the points on the graph lie along straight lines the propagation velocity of the pressure wave is constant along the path, an indication that each point along the soil path contributes equally to the total lag time (*i.e.*, the weighting factor is constant along the path). For the vertical path of Figure 5b, the weighting factor decreases with proximity to the soil surface. This is because the wave front velocity increases as it approaches the surface, decreasing the relative contribution of this part of the path to the total measured lag time.

The ideal for determining effective permeabilities over long paths is to have the weighting factor remain constant. In order to compare the effective weighting functions of the static measurement techniques with the vertical and horizontal measurements of the dynamic technique, we have plotted in Figure 6 the normalized weighting factors for the three measurements, for the configuration indicated in Figure 5b. The traces are normalized such that the weighting equals one at the surface of the pressure source (r=0.1 m). The weighting factors for the dynamic measurements are simply the slopes of the traces in Figure 5b. The weighting factor for the static case is proportional to 1/r. Even for the vertical path, the weighting factor for the dynamic measurement does not fall off nearly as sharply moving away from the probe as it does for the static measurement.

The apparent existence of scale dependence of soil permeability evident from the field tests of the dynamic technique is an important result. If this effect is verified by future tests, it means that the typical method of characterizing soil by multiple small-scale measurements can produce misleading results. A study by Schery and Siegel in a study of natural soil in Socorro, New Mexico(18), supports our finding of increasing permeability with scale. In one-dimensional tests of vertical permeability they found a factor of 20 increase in permeability as the

integration path increased from a few centimeters to about one meter. The authors showed evidence that increasing permeability with increasing scale resulted from the higher probability of intercepting spatially infrequent, high-flow paths at larger scales.

The ability to make not only larger scale measurements, but also measurements at different scales with one technique, is clearly an advantage for studying the transport characteristics of soils if scale dependence is typical—an issue that can be resolved by investigations in different soils using the dynamic technique. This feature, along with the ability to detect anisotropy make the technique desirable despite its drawback of being considerably more equipment intensive than the static methods.

Examination of the theory for estimating permeabilities from the static method elucidates an additional advantage in the present technique. Permeability is estimated from static measurements using an equation of the form:

$$k = \frac{Q\mu}{S\Delta P} \tag{21}$$

where Q is the steady flow imposed into or out of the probe, ΔP is the disturbance pressure difference between the surface and the sampling region of the probe (i.e., the total pressure difference minus the hydrostatic component), and S is a 'shape factor' that depends on the geometry of the probe. In the case of a buried cylinder, there is more than a factor of two range in published estimates of the shape factor (compare (19) and (20)). In addition, one source (20) shows a factor of 2 change in shape factor with probe depth, going from 0.15 m to 1.81m, while another is (19) is relatively insensitive to depth, giving only a 10% change in shape factor over the same depths. Our numerical estimates of the shape factor, used for the analysis of the static measurements given here, give a midrange value that is relatively insensitive to depth.(5) Data analysis for the probe-to-probe dynamic pressure technique does not require the use of a shape factor and therefore reduces the associated uncertainty.

An issue was raised in the theory section about the extent of the problem that is created by interpreting experimental data for heterogeneous or anisotropic soils using a homogeneous, isotropic model. All measurements of soil permeability rely on models for interpretation of experimental data. As with any other technique, the extent to which actual soils violate the model assumptions determines the accuracy of the technique. In this regard the current experimental technique does, however, improve on most previous techniques in two ways. First, the dynamic technique provides valuable information about relative permeabilities in specific directions since the end points of the path are well defined. This is not true of any single-probe technique, since the dominant information will come from the path of least resistance, but there is no way of

determining where the path lies. Second, the existence of systematic heterogeneity or anisotropy is immediately evident from the array of measurements, so if more detailed information on the soil is required one can improve on the solution by iterating a numerical model incorporating the guessed anisotropy or heterogeneity against the experimental results. The iterative procedure is likely to be extremely time intensive, however, and requires the availability of a model that can simulate anisotropy and layering and the time dependent boundary conditions desribed in the theory section.

Conclusions

We have described a method for measuring soil permeability to air on a scale of several meters. This is a particularly important scale for assessing soil permeability characteristics in investigations of the entry of soil-gas-borne contaminants into houses, because this tends to be the scale over which houses draw pollutants from the soil. Our dual-probe, dynamic pressure technique has a number of advantages over previous static and dynamic techniques for measuring permeabilities at this scale.

The primary improvement over the static technique stems from the fact that the parameter used for detection (the propagation velocity of the pressure signal) is relatively constant with distance from the signal source. Relatively unweighted measurements can therefore be made over longer path lengths than with prior techniques giving a better determination of effective permeability over the path. Comparison between the results of the smaller-scale, static permeability measurements and the longer-path-length dynamic measurements appear to indicate scale-dependence of soil permeability to air at the field test site. The dynamic results yield consistently higher permeabilities, with considerably less special heterogeneity, than the static measurements—on average by a factor of about six. This finding of scale-dependent permeability is further supported by the fact that the highest permeabilities of the dynamic measurements occurred in the two measurements with the longest paths.

These results indicate the need to sample soil systems over the scale at which advective flow naturally occurs for the system under study. For applications in which it is critical to determine the transport characteristics of soil over several meters, the advantages of the probe-to-probe technique over the static technique far outweigh the disadvantages of greater complexity in instrumentation and data analysis. Indeed attempting to characterize soils by using averages of multiple smaller-scale measurements could produce seriously misleading results.

The probe-to-probe technique also offers several advantages over the previously used dynamic pressure technique that relies on barometric pressure fluctuations for the source signal (13, 18): Our measurement is not confined to the vertical direction, but can be made along any arbitrary path from the source, allowing the

detection of anisotropy of soil permeability. The use of the controlled source signal enables integration of the detected signal over arbitrary long times greatly increasing the signal to noise ratio. The single-frequency source signal also allows frequency-sensitive detection, which limits the uncertainty in the propagation time (the indicator of permeability) to the frequency band width of the Fast Fourier Transform. The band width of the frequency channels are in turn determined by the data sampling frequency and experiment duration--both controllable parameters. In addition, manipulation of the source signal allows us to make measurements over longer path lengths and under wider range of soil conditions, greatly reducing uncertainty and increasing range relative to the previous dynamic technique.

Because the dual-probe dynamic technique not only allows the measurement of soil permeability to air over larger scales than previously used *in situ* techniques, but also over a range of scales using the same technique, it promises to be an important tool for improving our understanding of gas-phase contaminant transport in soils. We plan to use the technique to further test the scale-dependence of permeability indicated by the field test. Such an effect could explain the large and persistent discrepancy between measured and modeled entry of radon-bearing soil-gas into houses.

Acknowledgments

We would like to thank John Wooley and Marc Fischer for their help on the field tests and Kenneth Revzan for providing the numerical simulation of the cylindrical probe. We also thank William Fisk, Ashok Gadgil, and Yvonne Tsang for their valuable review comments. This work was supported by the Director, Office of Energy Research, Office of Health and Environmental Research, Environmental Sciences Division, and by the Assistant Secretary for Conservation and Renewable Energy, Office of Building and Community Systems, Building Systems and Materials Division of the U.S. Department (DOE), under Contract DE-AC03-76SF00098.

Literature Cited

1. Garbesi, K.; Sextro, R. G. *Environmental Science and Technology* **1989,** 23, 1481.
2. Turk, B. H.; Prill, R. J.; Grimsrud, D. R.; Moed, B. A.; Sextro, R. G. *Journal of the Air and Waste Management Association* **1990,** 40, 498.
3. Hodgson, A. T.; Garbesi, K.; Sextro, R. G.; Daisey, J. M. *Journal of the Air and Waste Management Association* **1992,** 42, 277.
4. Garbesi, K.; Sextro, R. G.; Fisk, W. J.; Modera, M. P.; Revzan, K. L. *Soil-Gas Entry into an Experimental Basement: Model-Measurement Comparisons and Seasonal Effects;* Technical Report No.; Lawrence Berkeley Laboratory: Berkeley, CA: 1992.
5. Fisk, W. J.; Modera, M. P.; Sextro, R. G.; Garbesi, K.; Wollenberg, H. A.; Narasimhan, T. N.; Nuzum, T.; Tsang, Y. W. *Radon Entry into Basements: Approach, Experimental Structures, and Instrumentation of the Small Structures Project;* Technical Report No.; Lawrence Berkeley Laboratory: Berkeley, CA: 1992.
6. Nazaroff, W. W.; Lewis, S. R.; Doyle, S. M.; Moed, B. A.; Nero, A. V. *Environ. Sci. Technol.* **1987,** 21, 459.
7. De Boodt, M. F.; Kirkham, D. *Soil Science* **1953,** 76, 127.
8. Tanner, A. B. *Methods of Characterization of Ground for Assessment of Indoor Radon Potential at a Site.* in *Field Studies of Radon in Rocks, Soils, and Water.* 1991. U.S. Geological Survey Bulletin.
9. Bear, J. *Dynamics of Fluids in Porous Media,* ed.; Dover Publications Inc.: New York, 1972,
10. Carslaw, H. S.; Jaeger, J. C. *Conduction of Heat in Solids,* 2nd ed.; Clarendon Press: Oxford, 1959,
11. Beck, J. V.; Cole, K. D.; Haji-Sheikh, A.; Litkouhi, B. *Heat Conduction Using Green's Function,* ed.; Hemisphere Publishing Corp.: London, 1992, 523.
12. Brimhall, G. H.; Lewis, C. J. *Differential Element Transport in the Soil Profile at the Ben Lomond Small Structure Radon Site: A Geochemical Mass Balance Study;* Technical Report No.; Department of Geology and Geophysics, University of California, Berkeley: 1992.
13. Fukuda, H. *Soil Science* **1955,** 4, 249.
14. Fisk, W. J., *et al. Monitoring and Modeling for Radon Entry into Basements: A Status Report for the Small Structures Project;* Technical Report No.; Lawrence Berkeley Laboratory: Berkeley, CA: 1989.
15. Garbesi, K. *Experiments and Modeling of the Soil-Gas Transport of Volatile Organic Compounds into a Residential Basement;* Technical Report No.; Lawrence Berkeley Laboratory: 1988.
16. Freeze, R. A.; Cherry, J. A. *Groundwater,* ed.; Prentice-Hall, Inc.: Englewood Cliffs, New Jersey, 1979,
17. Weeks, E. P. *Field Determination of Vertical Permeability to Air in the Unsaturated Zone;* Technical Report No.; United States Government Printing Office, Washington, DC: 1978.

18. Schery, S. D.; Siegel, D. *Journal of Geophysical Research* **1986,** 91, 12366.
19. Hahne, E.; Grigull, U. *Journal of Heat and Mass Transfer* **1975,** 18, 751.
20. Holman, J. P. *Heat Transfer*, ed.; McGraw Hill: New York, 1976,

Figure Captions

Figure 1. Geometry for the real and image sources and two possible probe locations.

Figure 2. Sample theoretical curves of time lag vs. permeability for a source at depth (L) = 2 m with a source signal period of 60 s. Traces are for different possible detector locations, given by radial distance (r) and angle (θ), as in Figure 1.

Figure 3. Permeabilities measured at each of the detector probes (in parentheses) using the static technique, and for each pathway between the source and detector probes (in square brackets) using the dynamic technique. Probe IDs as in Table I.

Figure 4. Schematic of experiment design. On the three-way solenoid valves, the ports are marked 'c' for common, and '*' for the port that is opened at t = 0 for directing the signal to the source and detector probes. The venting solenoids are included to ensure that the source probe pressure is neutral up until t = 0. The ports marked 'cal & zero' or for checking the calibration and zero settings on the pressure transducers.

Figure 5 (a) Lag time of signal with distance from source along a horizontal ray ($\theta = 0^o$, Figure 1) and a vertical ray ($\theta = 90^o$) for a soil with permeability 8.5×10^{-13} m^2 and source at depth (L) = 2 m. (b) Same as Figure 3a, except for a soil with permeability 8.5×10^{-12} m^2 and source at depth (L) = 2 m.

Figure 6. Weighting factors of soil as a function of distance from the source probe for the horizontal and vertical path measurements indicated in Figure 5b, and for a static pressure measurements. The source probe is assumed to be at depth (L) = 2 m.

Table I. Permeabilities (k) determined at the probes using static techniques and between the reference and detector probes using the dual-probe dynamic technique.

Probe ID[a]	r and θ as in Figure 1	Static Detector Probe k (10^{-12} m^2)[b]	Static Source Probe k (10^{-12} m^2)	Avg. of static k at end points[c] (10^{-12} m^2)	Dynamic k of path[d] (10^{-12} m^2)	Ratio of dynamic to avg. static	Dynamic Regional Avg. k (10^{-12} m^2)
SE-S	2.0 m, 45°	1.6 ± 0.1	5.9 ± 0.4	3.8	17±1.3	4.5	
SW-S	2.0 m, 45°	4.9 ± 0.4	5.9 ± 0.4	5.4	15±1.3	2.8	
NW-S	2.0 m, 45°	1.6 ± 0.1	5.9 ± 0.4	3.8	18±1.4	4.7	17
N-M[d]	3.1 m, 30°	9.8 ± 0.7	5.9 ± 0.4	7.9	35±2.0	4.4	35
E-D	2.0 m, 0°	0.53 ± 0.04	5.9 ± 0.4	3.3	25±1.6	7.6	
S-D	2.0 m, 0°	0.29 ± 0.02	5.9 ± 0.4	3.1	23±1.5	7.4	
W-D	2.0 m, 0°	0.82 ± 0.06	5.9 ± 0.4	3.4	22±1.5	6.5	23
N-D[d]	2.6 m 0°	3.6 ± 0.2	5.9 ± 0.4	4.8	29±1.8	6.0	29

[a]The part of the probe ID coming before the dash is the compass direction, SE=southeast, etc., the part coming after the dash is the depth, S=shallow, M=mid-level, D=deep. The source probe is at the D level.

[b]Uncertainties, calculated assuming shape factor is certain, are based on environmental noise in measurements, which exceeds uncertainty due to propogation of instrumental errors.

[c]Average of the static measurements of permeabilities at the source and detector probes.

[d]Estimated permeability of the path between the source and detector probes determined from the dynamic pressure technique using the model described by Equations 13 - 15. Uncertainties derived from uncertainty in measurement of air-filled porosity of soil and uncertainty in time lag.

Figure 1.

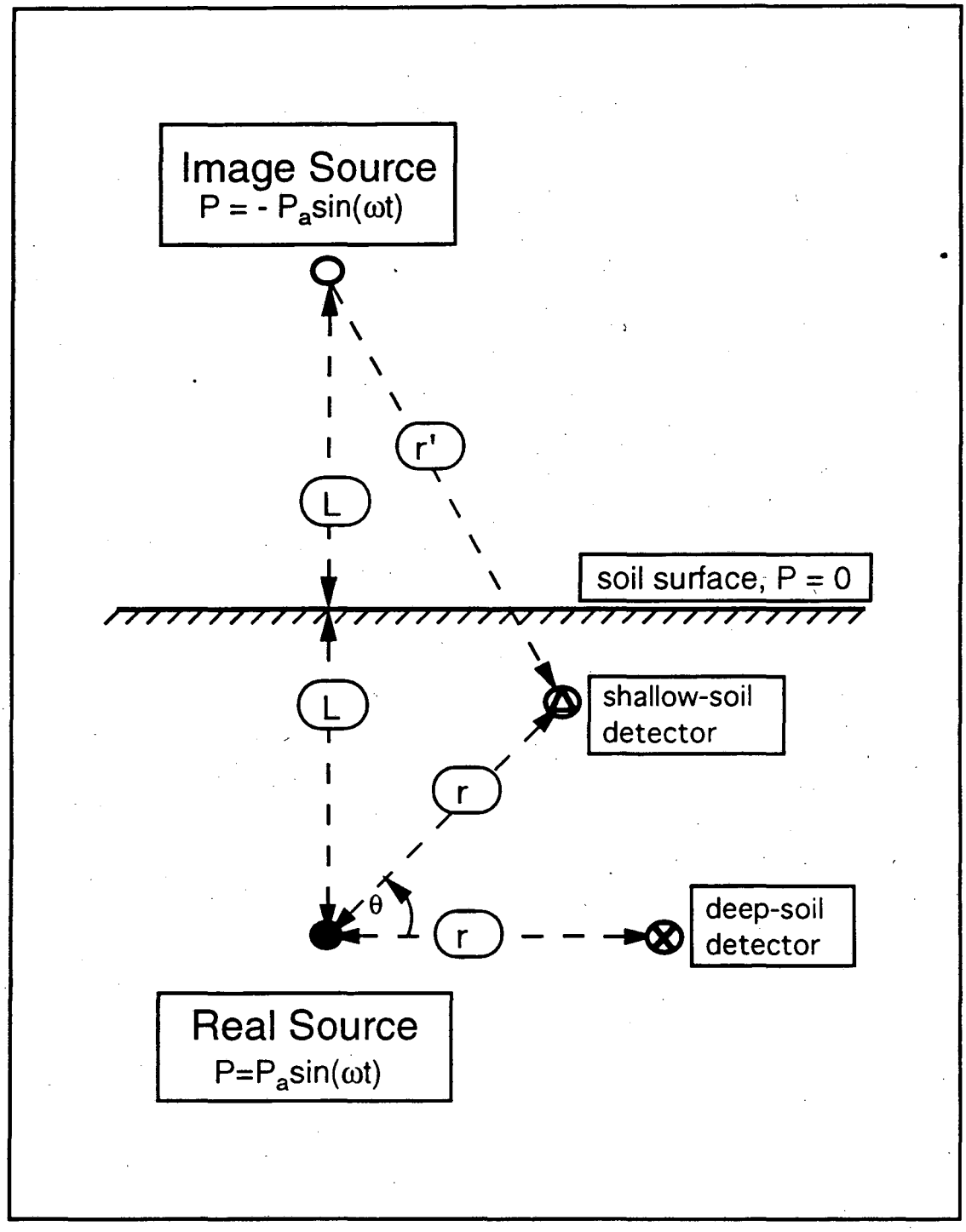
Image Source
P = - P$_a$sin(ωt)
r'
L
soil surface, P = 0
L
shallow-soil detector
r
θ
r
deep-soil detector
Real Source
P=P$_a$sin(ωt)

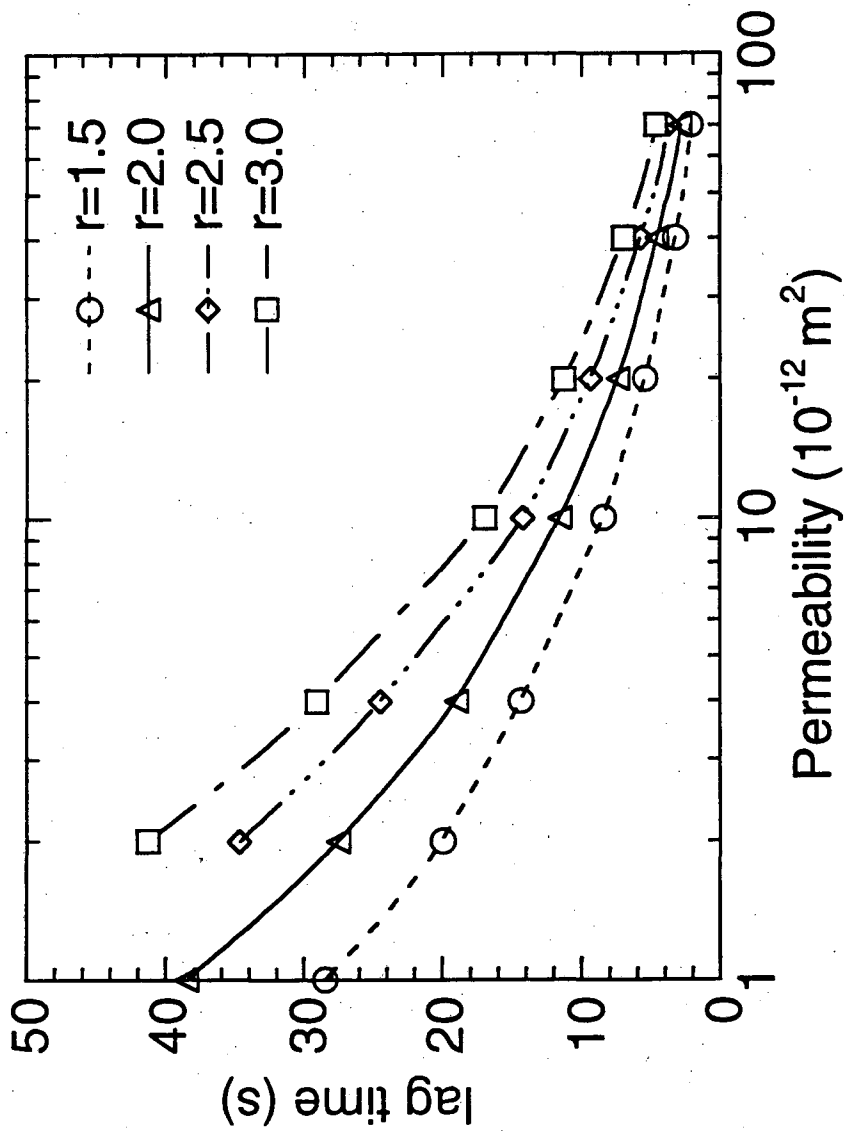
r=1.5
r=2.0
r=2.5
r=3.0
lag time (s)
Permeability (10^{-12} m^2)
0
10
20
30
40
50
1
10
100

Figure 2.

Figure 3.

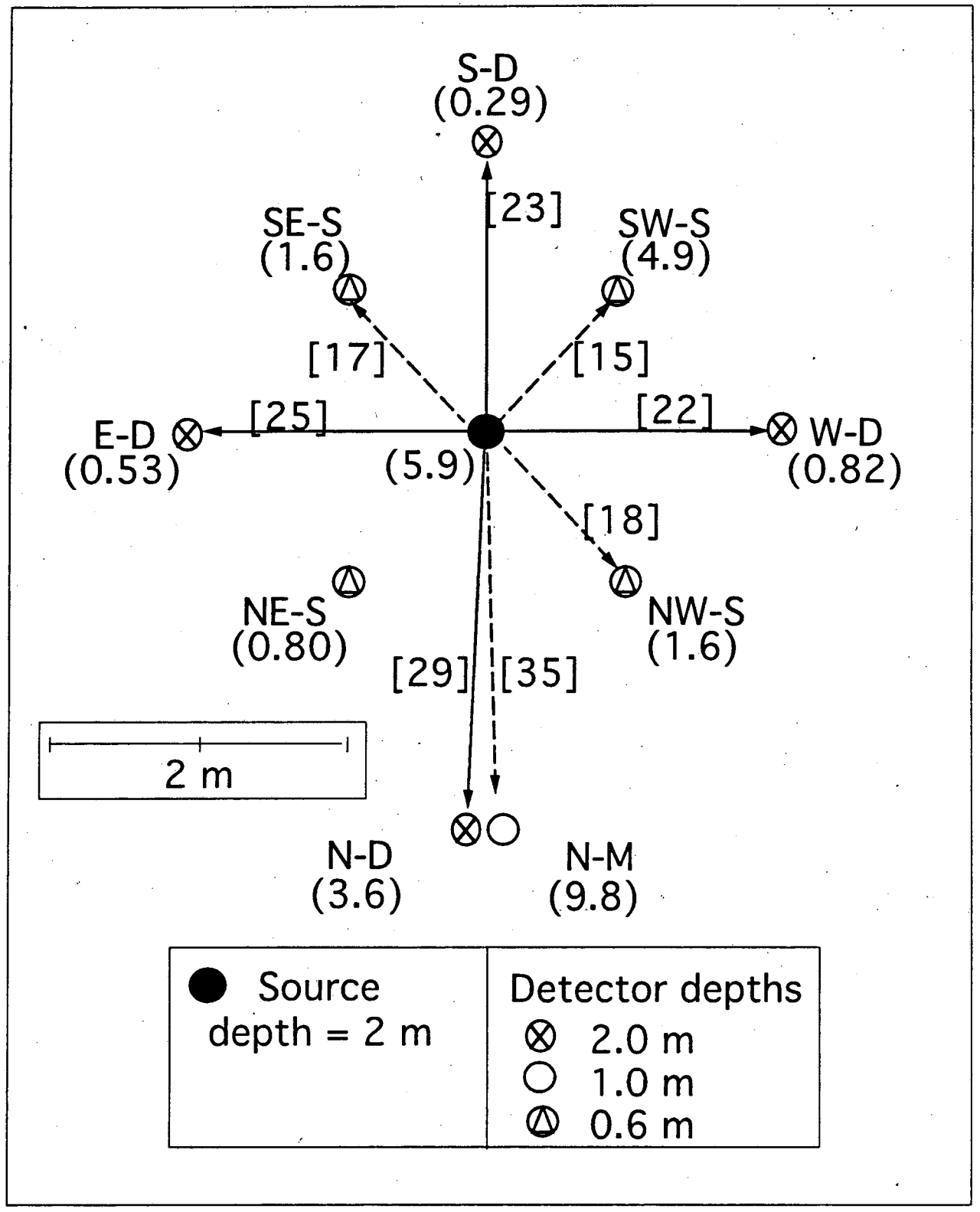
S-D
(0.29)
[23]
SE-S
(1.6)
SW-S
(4.9)
[17]
[15]
[25]
[22]
E-D
(0.53)
(5.9)
W-D
(0.82)
[18]
NE-S
(0.80)
NW-S
(1.6)
[29]
[35]
2 m
N-D
(3.6)
N-M
(9.8)
Source
depth = 2 m
Detector depths
2.0 m
1.0 m
0.6 m

Figure 4.

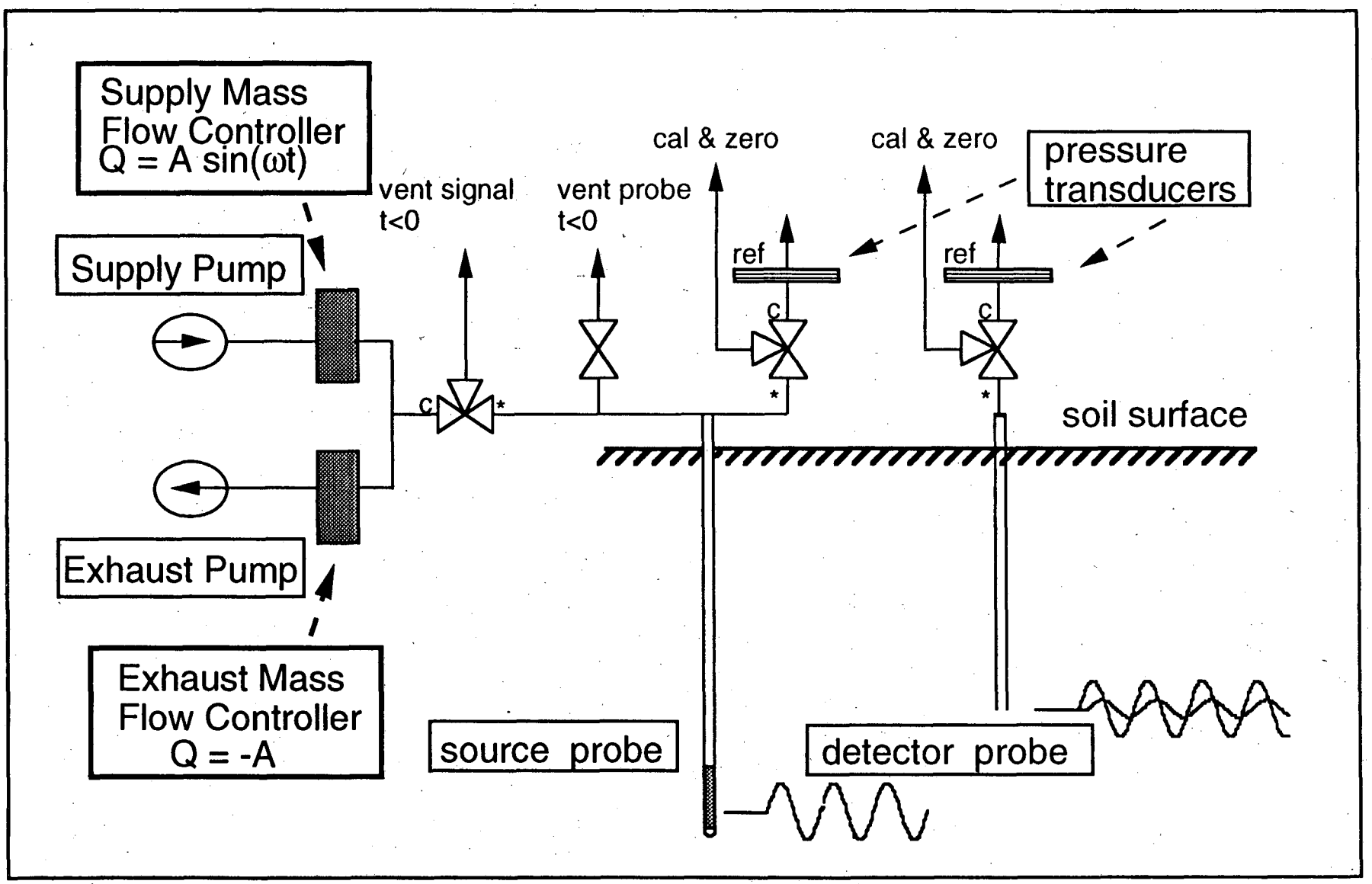
Supply Mass Flow Controller Q = A sin(ωt)
Supply Pump
Exhaust Pump
Exhaust Mass Flow Controller Q = -A
vent signal t<0
vent probe t<0
cal & zero
cal & zero
pressure transducers
ref
ref
c
c
c
*
*
*
soil surface
source probe
detector probe

Figure 5 (a) and (b).

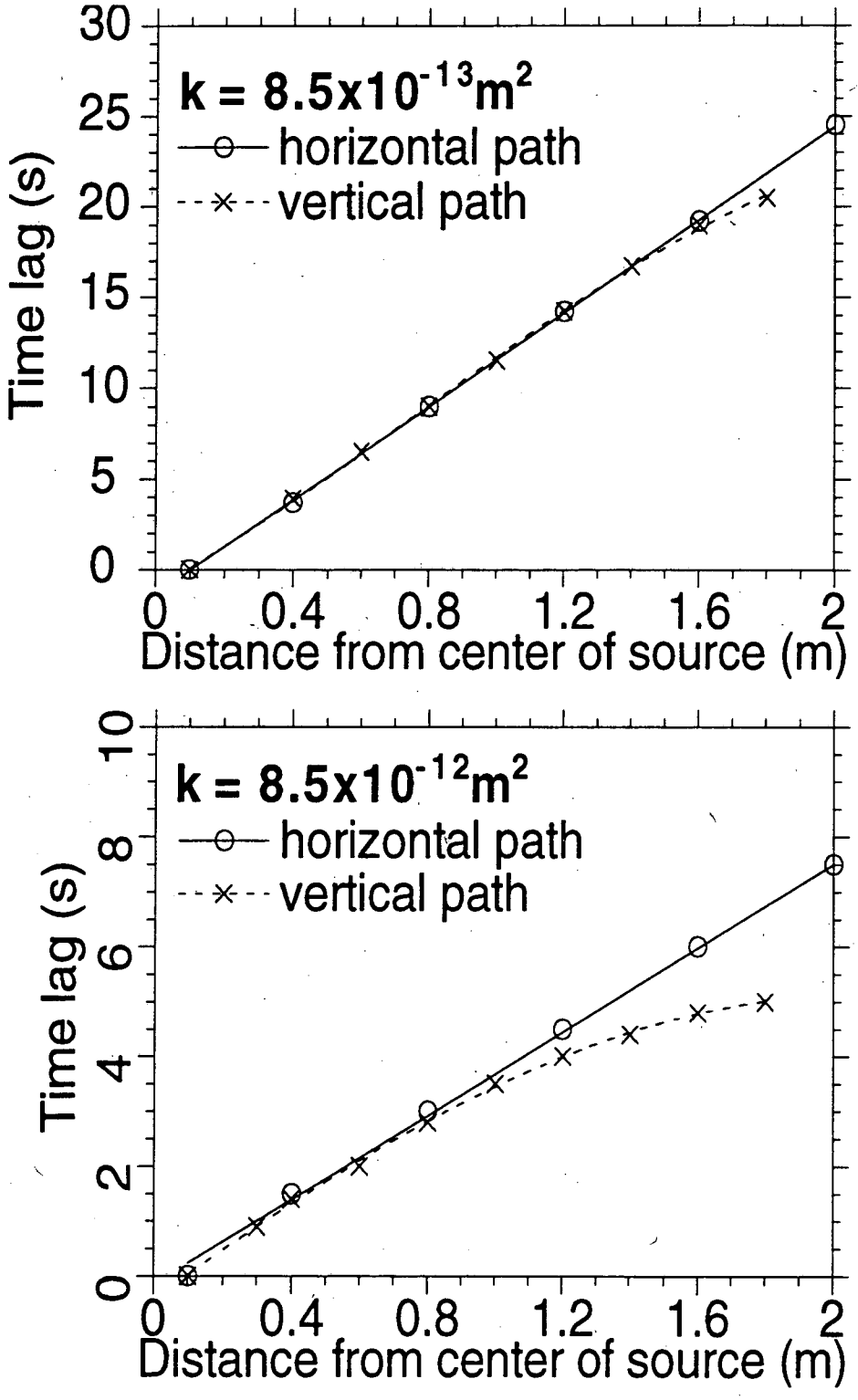

Figure 6.

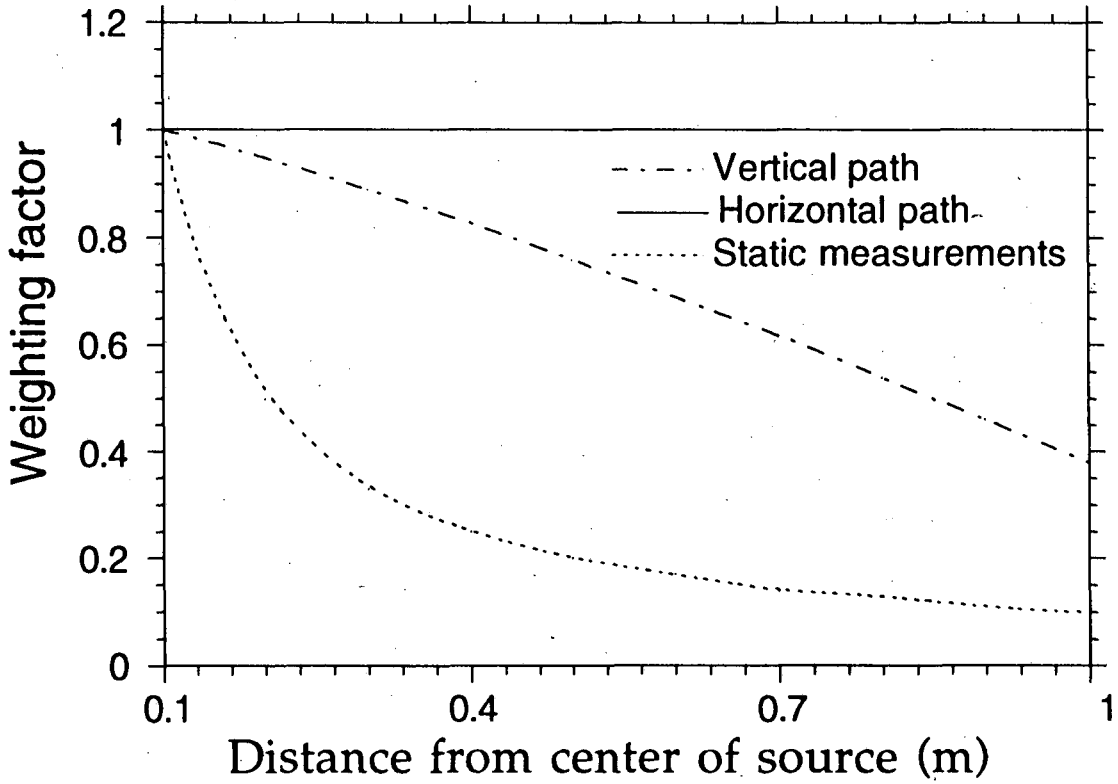
1.2
1
0.8
0.6
0.4
0.2
0
Weighting factor
Vertical path
Horizontal path
Static measurements
0.1
0.4
0.7
1
Distance from center of source (m)

LAWRENCE BERKELEY LABORATORY
UNIVERSITY OF CALIFORNIA
TECHNICAL INFORMATION DEPARTMENT
BERKELEY, CALIFORNIA 94720